KIEE International Transactions on Electrical Machinery and Energy Conversion Systems, Vol. 5-B No. 2, pp. 103~110, 2005 103

Monolith and Partition Schemes with LDA and Neural Networks as Detector Units for Induction Motor Broken Rotor Bar Fault Detection

Bulent Ayhan*, Mo-Yuen Chow* and Myung-Hyun Song*

Abstract - Broken rotor bars in induction motors can be detected by monitoring any abnormality of the spectrum amplitudes at certain frequencies in the motor current spectrum. Broken rotor bar fault detection schemes should rely on multiple signatures in order to overcome or reduce the effect of any misinterpretation of the signatures that are obscured by factors such as measurement noises and different load conditions. Multiple Discriminant Analysis (MDA) and Artificial Neural Networks (ANN) provide appropriate environments to develop such fault detection schemes because of their multi-input processing capabilities. This paper describes two fault detection schemes for broken rotor bar fault detection with multiple signature processing, and demonstrates that multiple signature processing is more efficient than single signature processing.

Keywords: Induction motor, broken rotor bars, fault detection, Multiple Discriminant Analysis, Artificial Neural Networks, Multiple signature processing.

1. Introduction

Induction motors have dominated the field of electro-mechanical energy conversion, being 80% of the motors in use [1]. The applications of induction motors are widespread. Some induction motors are key elements in assuring the continuity of the process and production chains of many industries. A majority of induction motors are used in electric utility industries, mining industries, petrochemical industries, and domestic appliances industries. The list of the industries and applications that induction motors take place in is rather long. Induction motors are also often used in critical applications such as nuclear plants, aerospace, and military applications, where the reliability must be of high standards.

Induction motors often operate in hostile environments such as corrosive and dusty places. They are also exposed to a variety of undesirable conditions and situations such as misoperations. These unwanted conditions can cause the induction motor to go into a premature failure period, which may result in an unserviceable condition of the motor, if not detected at its early stages of the failure period. The failure of induction motors can result in a total loss of the machine itself, in addition to a likely costly downtime of the whole plant. More importantly, these failures may even result in the loss of lives, which cannot be tolerated. Thus, health monitoring techniques to prevent induction motor failures are of great concern in industry and are gaining increasing attention [2]-[3]. Rotor failures are among these failures, and they now account for 5-10% of total induction motor failures[4]. Several monitoring techniques have been developed, most of which are based on motor current signature analysis (MCSA). In recent years, several advanced signal processing techniques such as High Resolution Spectral Analysis, Higher Order Statistics, and Wavelet Analysis have been applied to broken rotor bar and other motor fault detection problems [1].

Broken rotor bar fault in induction motors can be detected by monitoring any abnormality of the motor current power spectrum amplitudes at several certain frequency components. These frequency components are located around the main frequency line and are determined according to the number of poles and mechanical speed of the motor. However, there are other effects that may obscure the detection of the broken rotor bar fault or cause false alarms. For example, these effects can be intrinsic manufacturing dissymmetry [5], or load torque oscillation that can produce stator currents with the frequency values the same as the monitored frequencies. A broken rotor bar fault detection scheme based on multiple frequency signatures thus should be more reliable in overcoming or reducing the effect of misinterpreted signatures, which are caused by the effects discussed formerly or some other unknown reasons. Multiple Discriminant Analysis(MDA) and Artificial Neural Networks (ANN) provide appropriate environments to develop such fault detection schemes because of their multi-input processing capabilities.

This paper presents two fault detection schemes for broken rotor bar fault detection with multiple signature processing and demonstrates that multiple signature processing is more effective than single signature processing. The first

* Box 7911 Flex Dept. of Electrical and Computer Engineering North Carolina State University Raleigh, NC 27695, USA (chow@ncsu.edu)
Received April 6, 2005 ; Accepted May 19, 2005

scheme will be named the "monolith scheme," and it is based on a single MDA or a single ANN unit representing the complete motor operating load torque region. The second scheme will be named the "partition scheme," and it consists of several small MDA or ANN units, each of which representing a particular load torque operating region. The two detection schemes have been investigated using experimental data with MDA and ANN detection units, respectively.

This paper is organized as follows: Section II discusses the frequencies of interest to the broken rotor bar problem and outlines the frequencies to be used in the MDA and ANN units. Section III presents the experiment setup and motor data specifications. Section IV outlines the fault detection schemes together with experimental results and analysis. Section V concludes the findings of this paper.

2. Motor Current Spectral Components for Broken Rotor Bar

Kliman, Thomson, Filipetti, Elkasabgy [6-7] used motor current signature analysis (MCSA) methods to detect broken rotor bar faults by investigating the sideband components around the supplied current fundamental frequency (i.e. the line frequency), f_o :

$$f_b = (1 \pm 2s) f_o , \tag{1}$$

where f_b are the sideband frequencies associated with the broken rotor bar, s is the per unit motor slip. The slip s is defined as the relative mechanical speed of the motor, n_m, with respect to the motor synchronous speed, n_s, as:

$$s = \frac{n_s - n_m}{n_s} . \tag{2}$$

The motor synchronous speed, n_s, is related to the line frequency f_o as:

$$n_s = \frac{120 f_o}{P} , \tag{3}$$

where P is the number of poles of the motor and the constant '120' is used to express the motor synchronous speed, n_s, in revolutions per minute (rpm) unit.

The broken bars also give rise to a sequence of other sidebands given by [7]:

$$f_b = (1 \pm 2ks) f_o , \quad k = 1, 2, ..., k_n \text{ where } f_b > 0 \ \forall k , \tag{4}$$

and is depicted conceptually in Fig. 1.

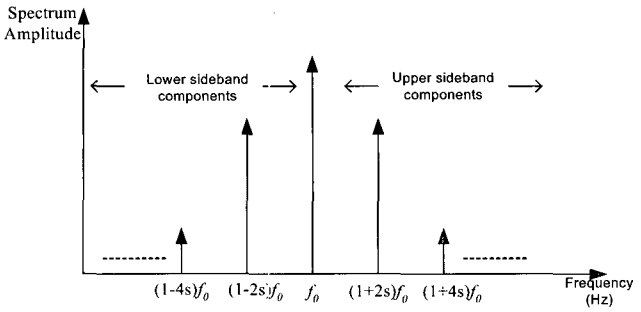

Fig. 1 Sideband frequencies around the fundamental line frequency.

Fig. 1 shows the frequency components specific to broken rotor bar fault, which is given in equation (4) for $k = 1$ and 2. These frequencies are located around the fundamental line frequency and are termed as lower sideband and upper sideband components as indicated in Fig 1. There are other spectral components that can be observed in the stator line current due to broken rotor bar fault [6]:

$$f_b = \left[\left(\frac{k}{p} \right) (1 - s) \pm s \right] f_0 , \text{ where } k/p = 1,3,5,\ldots . \tag{5}$$

The fault detection schemes investigated in this paper depend on multiple signature processing. These signatures correspond to the power spectrum amplitudes of the motor current (phase-a) data at the selected frequencies. A detailed explanation about the experiment setup and specifications of the collected motor data will be given in Section III. We use Welch's periodogram method to compute the power spectrum of phase-a motor current data. In Welch's periodogram method, we apply a Hanning window and 50% overlapping percentage among the partitioned segments. It has been noted that the use of a Hanning window and 50% overlap leads to an efficient implementation of the FFT algorithm [8]. In the fault detection schemes, we consider four of the broken rotor bar fault specific frequency components. Let $\mathbf{F} = \{f_{1^-}, f_{1^+}, f_{2^-}, f_{2^+}\}$ be the set of broken rotor bar fault specific frequency components, and $\mathbf{P} = \{p_{1^-}, p_{1^+}, p_{2^-}, p_{2^+}\}$ be the set of Welch's spectrum amplitudes at these frequencies. The frequency components in set **F** are: $f_{1^-} = (1 - 2s) f_0$, $f_{1^+} = (1 + 2s) f_0$, $f_{2^-} = (1 - 4s) f_0$ and $f_{2^+} = (1 + 4s) f_0$, where f_0 is the fundamental stator current frequency and s is the slip. f_{1^-} and f_{1^+} are the first lower and upper sidebands, while f_{2^-} and f_{2^+} are the second lower and upper sidebands around f_0, which are expressed mathematically in equation (4). The inputs for the

MDA and ANN units in the monolith and partition schemes thus consist of the signature set: $\{p_{1^-}, p_{1^+}, p_{2^-}, p_{2^+}\}$.

The motivation in choosing the first and second lower and upper sidebands around the fundamental supply frequency is due to higher signal to noise ratio of these harmonics, which contain more reliable and discriminative information when compared to other harmonics. The higher frequency harmonics are relatively low in spectrum amplitude; they are thus more sensitive to noise. However, there is no restriction in including other signatures or increasing the number of signatures within the investigated detection schemes, as far as the included signatures provide discriminative information about the broken rotor bar fault.

The methodology, in the investigated fault detection schemes, uses the Welch's spectrum amplitudes of motor current data at the broken rotor bar fault specific frequencies as the discriminative signatures in the fault detection decision. However, the locations of the monitored frequencies, f_b, depend on the slip factor, s, which is a function of the motor mechanical speed. When the no load case of motor is considered, the slip factor value approaches to 0. This results in the interference of the monitored frequencies with the main supply frequency or its harmonics. The current detection schemes will thus not be able to perform efficiently for the no load condition of the motor. On the other hand, signatures that are not dependent on the slip factor, and that carry discriminative information, can be included within the methodology in order to make the detection schemes provide reliable fault decision in the no load condition of the motor.

3. Experiment Setup and Motor Data Specifications

The characteristics of the 3-phase induction motor used in our experiment are listed in Table 1. The motor was tested with the healthy rotor and with the faulty rotor that had one broken rotor bar. The broken rotor bar fault was induced by filling one of the rotor bars full with anchoring cement before the die-casting process. Anchoring cement is a high strength, fast-setting gypsum cement with low conductivity. The overall data collection scheme and the actual experiment setup picture are depicted in Figures 2 and 3, respectively.

Table 1 Induction motor characteristics used in the experiment.

Description	Value
Power	0.75 kW (1Hp)
Input Voltage	380 V
Full Load Current	2.2 A
Supply Frequency	60 Hz
Number of Poles	4
Number of Rotor Slots	44
Number of Stator Slots	36
Full Load Torque	0.43 kg·m
Full Load Speed	1690 rpm

The induction motor was fed through a 3 phase ABB, ACS 501 inverter. A Tektronix TM 5003 current amplifier amplifies the induction motor stator currents before being sent to the interfacing Pentium PC through the oscilloscope. The needed load condition of the induction motor was established by connecting the test motor to a DC Motor, which is used as a generator and is capable of simulating any desired load condition. The speed of the induction motor was measured by a digital stroboscope.

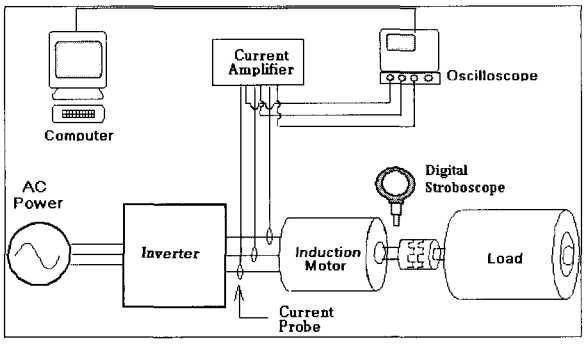

Fig. 2 Motor data collection scheme.

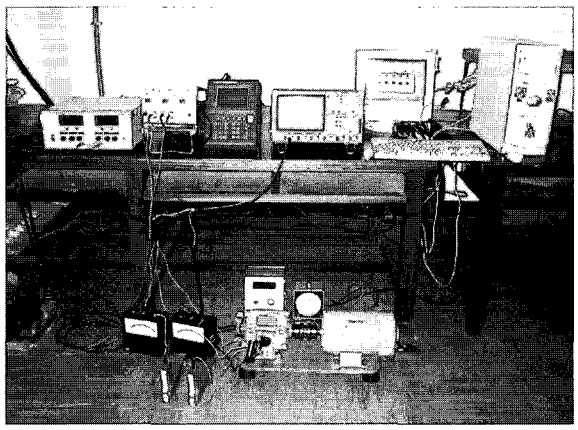

Fig. 3 Actual experiment setup to collect healthy and faulty motor data.

The experiments involved collecting three phase stator induction motor current and speed data for four different load conditions of the motor both with one broken rotor bar fault and without any fault. The load conditions of the motor are 25%, 50%, 75% and full load respectively. These load condition percentages are determined according to the motor nameplate information given in Table 1. Thus, there are a total of 8 different experiment cases. For each individual case, 20 sets of motor current data were collected. Each motor current data set contains 10,000 samples for a duration of one second, which makes the sampling frequency 10kHz. A sample phase-a motor current data

waveform corresponding to healthy state of motor under full load condition is demonstrated in Fig. 4.

4. Fault Detection Schemes and Experimental Results

Let C denote the motor condition, which is comprised of the two states of the motor: healthy condition, H, and faulty condition with one broken rotor bar, F, $C \in \{H,F\}$. From the motor current power spectrum analysis and broken rotor bar specific frequency components knowledge, there exists a mapping $\mathfrak{M}$ from $(\mathbf{P},T_L)$ to C as expressed in (6):

$$\mathfrak{M}:(\mathbf{P},T_L)\rightarrow C, \tag{6}$$

where $\mathbf{P}=\{p_{1^-},p_{1^+},p_{2^-},p_{2^+}\}$ is the set of Welch's periodogram power spectrum amplitudes at frequencies $\mathbf{F}=\{f_{1^-},f_{1^+},f_{2^-},f_{2^+}\}$ and T_L is the motor load condition. In our experiments, we have collected data at four different load conditions of the motor as discussed in Section III, where T_L is either at full load, 75%, 50% or 25% load, $T_L \in \{T_{L_{100\%}},T_{L_{75\%}},T_{L_{50\%}},T_{L_{25\%}}\}$. In these experiments, motor

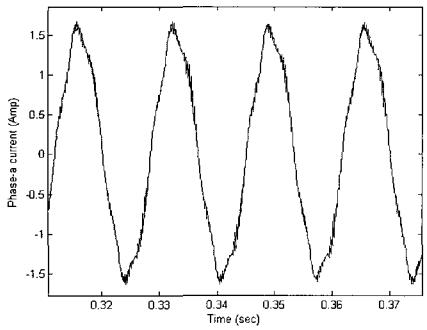

Fig. 4 Healthy phase-a motor current data collected from the experiment setup under full load condition of the motor.

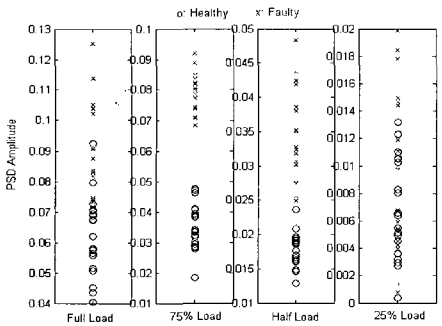

Fig. 5 PSD estimates at $f_{1^-}=(1-2s)f_o$ under motor load conditions: $T_L \in \{T_{L_{100\%}},T_{L_{75\%}},T_{L_{50\%}},T_{L_{25\%}}\}$.

speed variation in the collected motor speed data is less than 1.4% in all of the four investigated motor load conditions. Fig. 5 demonstrates the PSD estimates at one of the broken rotor bar fault specific frequencies, $f_{1^-}=(1-2s)f_o$, under four different motor load conditions: $T_L \in \{T_{L_{100\%}},T_{L_{75\%}},T_{L_{50\%}},T_{L_{25\%}}\}$.

In the monolith scheme, we use a single fault mapping unit, $\mathfrak{M}$, which maps the signatures extracted throughout the complete motor operating load condition, to the motor condition. This scheme is depicted in Fig. 6. Inputs of the fault mapping unit consist of the signature set $\{T_L,p_{1^-},p_{1^+},p_{2^-},p_{2^+}\}$, where T_L is the motor load condition, p_{1^-},p_{1^+} are the first and p_{2^-},p_{2^+} are the second lower and upper sidebands' Welch's periodogram power spectrum amplitudes around the fundamental current frequency, f_o, respectively. The mapping for the monolith scheme is depicted in (7):

$$\mathfrak{M}:(p_{1^-},p_{1^+},p_{2^-},p_{2^+},T_L)\rightarrow\{H,F\}. \tag{7}$$

In the partition scheme, the single mapping unit $\mathfrak{M}$, which is used in the monolith scheme, is divided into disjoint sub-mapping units $\mathfrak{M}_i$, where $\mathfrak{M}_i$ corresponds to a sub-mapping unit for a particular motor load condition and $\mathfrak{M}=\bigcup_{i=1}^{m}\mathfrak{M}_i$, $\bigcap_{i=1}^{m}\mathfrak{M}_i=\varnothing$. In our case, $m=4$. Thus, the sub-mapping units in the partition scheme consist of the spectrum amplitude signatures only. A sub-mapping unit is depicted in (8):

$$\mathfrak{M}_i:(p_{1^-},p_{1^+},p_{2^-},p_{2^+})\rightarrow\{H,F\}. \tag{8}$$

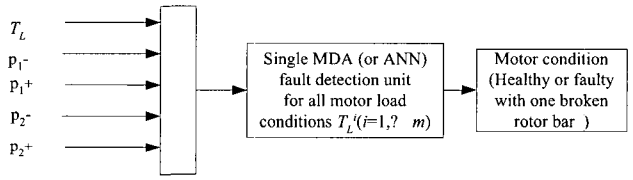

Fig. 6 The monolith scheme.

The conceptual diagram of the partition scheme is presented in Fig. 7. The mapping units in the partition scheme provide partitioning of the complete motor operating load region into subregions, each subregion corresponding to a constant load condition. This procedure thus transforms the nonlinear mapping problem into linear mapping problems or mapping problems with a lower order of nonlinearities. The partition scheme needs motor load condition information as a prerequisite for the preparation of the corresponding mapping units.

In our case, we partition the motor's load operating region into four subregions, depicted as $T_L = \{T_{L_{100\%}}, T_{L_{75\%}}, T_{L_{50\%}}, T_{L_{25\%}}\}$. We then form MDA and ANN units for each particular load subregion using the corresponding motor current signatures.

For analyses and performance comparisons of the fault detection schemes, two different cases are considered in this paper:

Case 1: Motor signature data set is treated as one whole training data set, where DataSet **D** = {Training Set} = {Test Set}.

Case 2: Motor signature data set is separated into two sets: training and test, where DataSet **D** = {Training Set} ∪ {Test Set} and {Training Set} ∩ {Test Set} = Φ.

Training process for the two cases consists of computing the coefficients of the linear discriminant functions for the MDA and the network weights for the ANN. Since we use linear discriminant functions we will call LDA instead of MDA in the remaining of this paper.

In the trials for finding proper ANN structures for both monolith and partition schemes, it is observed that there is a substantial range of ANN structures that can be selected among, which provide efficient and satisfactory performance. We have selected an ANN (5-10-1) structure for the large-scale unit in the monolith scheme and an ANN (4-5-1) structure to represent the small-scale units for each particular load condition in the partition scheme. In selection of these structures, we have taken into consideration that we have a larger number of units in the hidden layer than the input layer. The LM (Levenberg-Marquardt) training algorithm is used in both schemes.

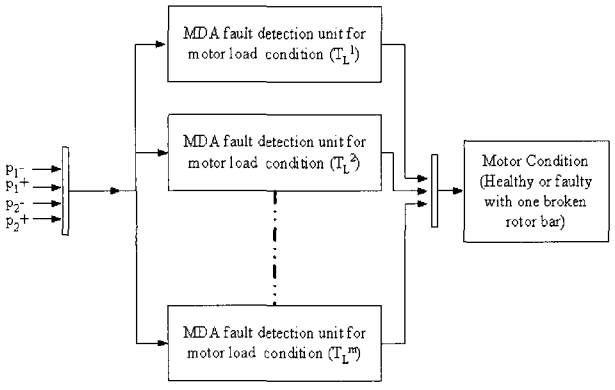

Fig. 7 The partition scheme.

In Case 1, we have stopped training if the network training error reaches a pre-set value, which in our case is 1e-5. In Case 2, we consider the same ANN structures but apply a different training stop technique, known as cross validation. Setting a fixed training error value to stop the training process may cause overtraining. Cross validation is a method to prevent overtraining. According to this technique, data are divided into two disjoint sets: The first data set is the training set, which is used for computing and updating the neural network weights and biases and the second set is used as the validation set [9].

We will also use the term test set as the validation set in our analyses. The error on the validation set is checked throughout the training process. It can be anticipated that the error in the validation set decreases during the initial steps of the training, just as the error in the training set. However, when the network begins to overfit the data in the training set, the error for the validation set begins to rise. When the validation error increases for a specified number of steps, the training is stopped to avoid overtraining, and the most recent weights and the biases are used as the neural network parameters [9]. Fig. 8 illustrates the principle of the cross validation technique. In this figure, it can be seen that training stops at the 12^{th} epoch, since the validation error corresponding to the validation set or test data set does not decrease, but slightly increases for some consecutive steps, while training error continually decreases.

In analyzing fault detection performances, we use statistical hypothesis testing, Type I error, α, and Type II error, β, which is expressed in Table 2. Our null hypothesis H_0:

H_0: Incoming motor signature test data correspond to healthy state of the motor.

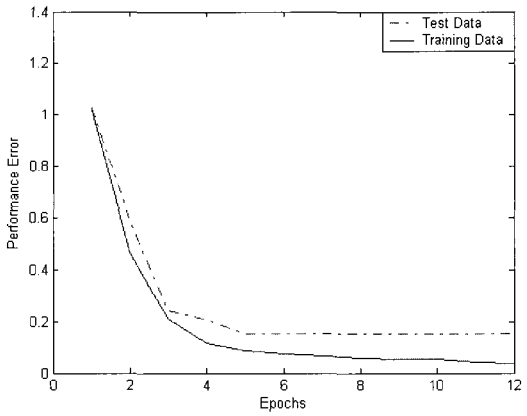

Fig. 8 Training and validation error curves with cross validation technique.

Type I error, α, will then correspond to the ratio of the healthy motor data, which are classified as faulty, to the total number of motor data. Likewise, Type II error, β, will correspond to the ratio of the faulty motor data, which are classified as healthy, to the total number of motor data. We will use the term 'Correct Detection Rate', CDR, in our analyses, which is mathematically expressed in (9):

$$\text{CDR} = (1 - \alpha - \beta). \tag{9}$$

Table 2 Type I and Type II Error Definition.

Decision	H_0 **is true**	H_0 **is false**
Reject H_0	Type I error	Correct
Do not reject H_0	Correct	Type II error

In order to compare the fault detection performances of single signature and multiple signature processing, we have applied LDA to each of the four signatures individually for both Case 1 and Case 2. Tables 3 and 4 depict the CDRs of each single signature under Case 1 and Case 2 together with Type I and Type II error measures. These tables indicate that CDRs change significantly according to each individual signature. Among these signatures, $(1-4s)f_o$ has the highest CDR, while the other three signatures have lower CDRs. The seventh to ninth rows of Table 4 simply sums CDRs and Type I-II errors of training and test data sets. We have then considered four of the signatures together and applied the monolith and partition schemes.

Table 3 CDRs of Single Frequency Components under Case 1.

	Correct Detection Rate (CDR)			
	$(1\text{-}2s)f_o$	$(1+2s)f_o$	$(1\text{-}4s)f_o$	$(1+4s)f_o$
CDR	132/160 =82.5%	150/160 =93.75%	152/160 =95.0%	117/160 =73.12%
Type I Error	10/160 =6.25%	2/160 =1.25%	1/160 =0.63%	21/160 =13.13%
Type II Error	18/160 =11.25%	8/160 =5.00%	7/160 =4.37%	22/160 =13.75%

Table 5 depicts the CDR of LDA and ANN for the two schemes under Case 1 together with Type I and Type II error measures. LDA's correct detection performance improves with the partition scheme. It is also observed that CDRs in both schemes are higher than any of the single signature's CDRs given in Tables 3 and 4.

The bar chart depicted in Fig. 9 presents the CDRs of both single signature processing and multiple signature processing for the two schemes under Case 1. This bar chart affirms that multiple signature processing is more efficient in broken rotor bar fault.

Table 6 depicts the CDRs and Type I-II errors of LDA and ANN under Case 2. In Case 2, since we have separated the data into training and test sets, we have included the sum of training and test data sets' CDRs, in addition to each set's separate CDR. There is a considerable improvement examined in the CDR with the partition scheme. In addition, these CDRs are higher than any of the single signature's CDRs that are depicted in Tables 3 and 4 with the exception of one equal case.

The partition scheme has provided an improved correct detection performance both in LDA and ANN. However, a significant performance increase is observed in LDA rather than ANN. This is because ANN has already given satisfactory response in the monolith scheme because of its nonlinear mapping and universal approximation capability. The partition scheme thus provides a way to cope with the nonlinearities in the mapping process especially for LDA. Partitioning the initial mapping space of the fault detection problem with respect to one of its input variables into smaller disjoint subregions and introducing sub-mapping units, either ANN or LDA, for each of these small subregions provide an increase in the correct detection performance.

Table 5 CDRs with Monolith and Partition Scheme under Case 1.

	Correct Detection Rate (CDR)	
	Monolith Scheme	Partition Scheme
CDR (LDA)	153/160=95.63 %	159/160=99.38 %
Type I Error (LDA)	1/160=0.63%	0/160=0.0%
Type II Error (LDA)	6/160=3.75%	1/160=0.63%
CDR (ANN)	160/160=100.0 %	160/160=100.0 %
Type I Error (ANN)	0/160=0.0%	0/160=0.0%
Type II Error (ANN)	0/160=0.0%	0/160=0.0%

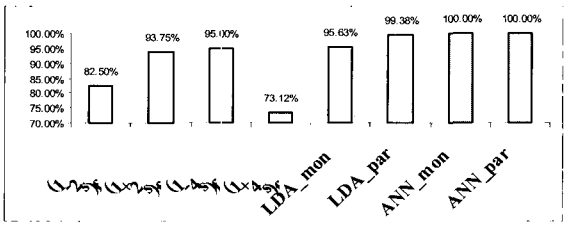

Fig. 9 CDRs with single signature processing and multiple signature processing under Case 1.

Table 4. CDRs of Single Frequency Components under Case 2.

	Correct Detection Rate (CDR)			
	$(1\text{-}2s)f_o$	$(1+2s)f_o$	$(1\text{-}4s)f_o$	$(1+4s)f_o$
CDR (Training)	72/80=90.00%	76/80=95.00%	75/80=93.75%	57/80=71.25%
Type I Error (Training)	4/80=5.00%	1/80=1.25%	1/80=1.25%	10/80=12.5%
Type II Error (Training)	4/80=5.00%	3/80=3.75%	4/80=5.00%	13/80=16.25%
CDR (Test)	61/80=76.25%	75/80=93.75%	77/80=96.25%	61/80=76.25%
Type I Error (Test)	4/80=5.00%	0/80=0.0%	0/80=0.0%	10/80=12.5%
Type II Error (Test)	15/80=18.75%	5/80=6.25%	3/80=3.75%	9/80=11.25%
CDR (Training+Test)	133/160=83.13%	151/160=94.38%	152/160=95.0%	118/160=73.75%
Type I Error (Training+Test)	8/160=5.00%	1/160=0.63%	1/160=0.63%	20/160=12.5%
Type II Error (Training+Test)	19/160=11.87%	8/160=5.00%	7/160=4.37%	22/160=13.75%

Table 6 CDRs with Monolith and Partition Schemes under Case 2.

	Correct Detection Rate (CDR)	
	Monolith Scheme	Partition Scheme
CDR (LDA – Tr)	76/80=95.00 %	80/80=100.0 %
Type I (LDA-Tr)	1/80=1.25%	0/80=0.0%
Type II (LDATr)	3/80=3.75%	0/80=0.0%
CDR (LDA - Test)	76/80=95.00 %	78/80=97.50%
Type I (LDA – Test)	0/80=0.0%	1/80=1.25%
Type II (LDA – Test)	4/80=5.0%	1/80=1.25%
CDR (LDA – Total)	152/160=95.00%	158/160=98.75%
Type I (LDA - Total)	1/160=0.63%	1/160=0.63%
Type II (LDA - Total)	7/160=4.37%	1/160=0.63%
CDR(ANN, Tr)	80/80=100.00%	80/80=100.0 %
Type I (ANN - Total)	0/80=0.0%	0/80=0.0%
Type II (ANN - Total)	0/80=0.0%	0/80=0.0%
CDR (ANN, Test)	78/80=97.50%	80/80=100.0%
Type I (ANN – Test)	2/80=2.5%	0/80=0.0%
Type II (ANN - Test)	0/80=0.0%	0/80=0.0%
CDR (ANN Tr +Test)	158/160=98.75%	160/160=100.0%
TypeI (ANN Tr + Test)	2/160=1.25%	0/160=0.0%
TypeII (ANN Tr+Test)	0/160=0.0%	0/160=0.0%

5. Conclusion

Multiple signature processing for broken rotor bar fault detection is considered to be more reliable than single signature processing because of the possibility of the obscuring effects that can overlap the significance of the one and only inspected signature. LDA and ANN provide a suitable environment to process multiple signatures for broken rotor bar fault detection. In this paper, we have demonstrated that multiple signature processing provides better accuracy with respect to fault detection performance when compared to single signature processing. In addition, we have investigated two fault detection schemes for broken rotor bar fault detection with multiple signature processing feature: the monolith and the partition schemes. Experimental results show that with the partition scheme, correct detection performance improves. The partition scheme reduces the dimension of the initial mapping space by partitioning it into smaller disjoint subregions. This, at the end, provides a better discrimination of broken rotor bar fault from the healthy state of the motor.

References

[1] M.E.H. Benbouzid , G.B. Kliman, "What stator current processing based technique to use for induction motor rotor faults diagnosis?," IEEE Power Engineering Review, August 2002.

[2] B. Li., M.-Y. Chow, Y. Tipsuwan, J.C. Hung, "Neural-network-based motor rolling bearing fault diagnosis," IEEE Trans. Industrial Electronics on , vol. 47, no. 5 , Oct. 2000, pp. 1060-1069.

[3] S. Altug, M.-Y. Chow, H.J. Trussell, "Fuzzy inference systems implemented on neural architectures for motor fault detection and diagnosis," IEEE Trans. on Industrial Electronics, vol. 46, no. 6 , Dec. 1999, pp. 1069 –1079.

[4] M. Haji, H. A. Toliyat, "Pattern recognition – a technique for induction machines rotor broken bar detection," IEEE Trans. on Energy Conversion, vol. 16, no. 4, Dec. 2001, pp. 312–317.

[5] A. Bellini, F. Filippetti, G. Franceschini, C. Tassoni, G.B. Kliman, , "Quantitative evaluation of induction motor broken bars by means of electrical signature analysis", IEEE Trans. on Industrial Applications, vol. 37, no. 5, Sep./Oct. 2001, pp. 1248-1255.

[6] G.B. Kliman et *al.*, "Non-invasive detection of broken rotor bars in operating induction motors", IEEE Trans. on Energy Conversion vol. EC-3, no. 4, pp. 873-879, 1988.

[7] F. Filipetti et *al.*, "AI Techniques in induction machines diagnosis including the speed rifle effect," IEEE- IAS Annual Meeting Conference, San Diego, pp. 655-662, Oct 6-10, 1996.

[8] S. Lawrence Marple, "Digital Spectral Analysis with Applications", Prentice Hall, 1987.

[9] S. Amari et *al.* "Asymptotic statistical theory of overtraining and cross validation," IEEE Trans. on Neural Networks, vol. 8, no. 5, Sep. 1997, pp. 985-996.

Bulent Ayhan (S-01)
He received the B.S. and M.S. degrees in electrical and electronics engineering from Bogazici University, Istanbul, Turkey, in 1998 and 2000 respectively. He is currently working toward the Ph.D. degree as a Research Assistant in Advanced Diagnosis Automation and Control Lab (ADAC) at North Carolina State University, Raleigh. His research interests include intelligent health monitoring of rotating machinery systems.

Mo-Yuen Chow (S'81–M'82–SM'93)
He received the B.S. degree in electrical and computer engineering from the University of Wisconsin, Madison, in 1982, and the M.Eng. and Ph.D. degrees from Cornell University, Ithaca, NY, 1983 and 1987, respectively. Upon completion of the Ph.D. degree, he joined the Department of Electrical and Computer Engineering, North Carolina State University, Raleigh and holds the rank of Professor since 1999. His core technology is diagnosis and control, artificial neural network and fuzzy logic with applications to areas including motors, process control, power systems and communication systems. He has established the Advanced Diagnosis Automation and Control (ADAC) Laboratory at NCSU.
Tel: (919) 515-7360, FAX: (919) 515-5108

Myung-Hyun Song
He was born in 1953 Jeju, Korea. He received the B.S., M.S., and Ph. D. degree in Electrical Engineering from Korea University, Seoul, Korea. Since 1988 he is Professor of School of Information & Communication Sunchon National University, Sunchon, Chonnam, Korea. From 1977-1981 he has industrial experience in the design and application of electric motor in Samsung Electronic Co., Suwon, Korea. His current research interests include induction motor fault detection & diagnosis, factory automation and web based control. He is a member of IEEE since 1995.